

Article

The Magnetic Band-Structures of Ordered $\text{Pt}_x\text{Fe}_{1-x}$, $\text{Pt}_x\text{Co}_{1-x}$, and $\text{Pt}_x\text{Ni}_{1-x}$ ($x = 0.25, 0.50$, and 0.75)

Ian Shuttleworth

School of Science and Technology, Nottingham Trent University, Nottingham NG11 8NS, UK;
ian.shuttleworth@ntu.ac.uk

Received: 21 October 2020; Accepted: 10 November 2020; Published: 13 November 2020



Abstract: The electronic band structures of the ordered $L1_2$ and $L1_0$ phases of the $\text{Pt}_x\text{M}_{1-x}$ ($M = \text{Fe}, \text{Co}$ and Ni) alloys were investigated using spin-polarized density functional theory (DFT). The relative contributions of both itinerant (Stoner) and localized magnetism at the high-symmetry k -points were determined and discussed qualitatively. Significant directional effects were identified along the A and R directions of the $L1_0$ and $L1_2$ alloys, respectively, and are discussed in terms of charge channeling effects.

Keywords: $\text{Pt}_x\text{Fe}_{1-x}$; $\text{Pt}_x\text{Co}_{1-x}$; $\text{Pt}_x\text{Ni}_{1-x}$; Stoner; itinerant; spin-polarized; band structure; density functional theory; DFT

1. Introduction

Magnetic alloys are a central class of materials whose importance is arguably as significant as their diversity. Studies of these alloys tend to focus these alloys in either thin-film or nanoparticle form [1,2] with applications in fields as diverse as medicine [3,4], magnetic media and devices [5], sensors [6,7] and catalysis [8–10]. Their importance derives from a number of factors. These include their ability to carry a magnetic moment and significantly the way that certain parameters can be tuned depending on how the alloy is prepared. This latter quality has had significant consequences, particularly in catalysis.

The $\text{Pt}_x\text{M}_{1-x}$ ($M = \text{Fe}, \text{Co}$ or Ni) alloys studied in the current work belong to a family of alloys that disorder at elevated temperatures but order at lower temperatures [11–13]. This structural complexity adds much to their significance because of the different properties the materials have depending on their short- and long-range order. For the alloys considered in the current work, these ordering effects can, for example, alter the optical [14], magnetic and structural properties [15–18], stress/strain relationships [19,20] and chemical reactivity [21] of the alloy. The stress–strain relationships in these alloys have recently shown [18,20] refs. therein] that these surfaces can be switched between mono-dentate and tri-dentate towards very common reaction species such as hydrogen and oxygen. The significance of this has only now started to be understood.

The structural diversity of Pt-based magnetic alloys [22] makes accurate computational and theoretical modeling challenging. Recent studies [23] have suggested that the magnetism of these systems may be a significant mechanism to explain the formation of the ordered phases of these alloys. However, a number of investigations exist to model and interpret the disordered phases of these alloys. Structurally, the formation of special quasirandom sequences [24] has simplified the process of sampling the inherently very large number of possible disordered structures for particular alloys and stoichiometries. The efficient modeling of the electronic band structures of these disordered structures is possible by embedding the coherent potential approximation (CPA) [25] into the Korringa–Kohn–Rostoker (KKR) approach, though more recent studies have started to use density functional theory (DFT) [26,27]. The CPA approximates the large unit cell of a disordered alloy with a smaller, ordered unit cell and then appropriately modifies the scattering potential at

each of the ordered lattice sites to simulate the disordered structure. Despite the successes of this approach, first-principles studies of the electronic band structures of the ordered alloys are starting to be developed [14,28,29]. The studies can provide highly accurate predictions for the ordered band structures, and recent studies in the field have estimated the importance of post-DFT approaches to these predictions [30]. These studies complement those performed using CPA–KKR and are less reliant on factorization, though they are limited by their computational cost.

The underlying theme in these previous studies has been their extensive treatment of the solution, or amorphous, phases of the bimetallic alloys. This accompanies the extensive applied interest in these materials, which has guided many contemporary investigations in the field where the primary focus has been the solution phase. In the current work, the focus is on the band structures of the ordered phases of Pt–Ni, Pt–Fe and Pt–Co alloys and in which case the most significant comparable studies are the recent theoretical investigations of M_xPt_{1-x} , ($M = \text{Co, Ni}$) [29] and of Ni_xPt_{1-x} [30] and the more established experimental studies of Ni_3Pt and $NiPt_3$ [31]. The importance of ordered phase studies as a contribution to the theoretical description of these magnetic bimetallic materials is because they remove the level of approximation required to describe a disordered, or mixed phase, material. This level of approximation is required in, for example, the CPA described in the previous paragraph. Further, it establishes a computational framework around which a more thorough theoretical description of these alloys may become possible, and ideally, these developments will be accompanied by appropriate experimental studies of the ordered crystalline systems.

Computationally, increasing the level of order or crystallinity means that more ab initio approaches can be used. It has been outlined earlier in this section that theoretical investigations into these bimetallic alloys have been dominated by the CPA. The reason for this has been because the very large majority of the available experimental data and of the useful applications of these materials have focused on disordered samples. For disordered systems, the CPA [32] has been developed as the most appropriate computational tool, as is it computationally feasible for systems seen experimentally. The CPA requires parametrization, which draws it away from the more ab initio ideals present in, for example, density functional theory (DFT). The current theoretical interest is in the application of DFT and post-DFT methods to these systems, and there have been recent [30] quasiparticle (i.e., post-DFT) investigations of Pt_xNi_{1-x} . However, in terms of purely characterizing materials and mechanisms, the DFT is still very much the accepted level of theory.

In the current work, the spin-resolved electronic band structures of the ordered Pt_xM_{1-x} ($M = \text{Fe, Co and Ni}$; $x = 0.25, 0.50$ and 0.75) alloys are investigated using DFT. The band structures will be elucidated and discussed in terms of the magnetic moment distribution through reciprocal space.

2. Results

The geometric structures of the ordered $Pt_{0.75}M_{0.25}$ ($M = \text{Fe, Co or Ni}$) and $Pt_{0.5}M_{0.5}$ alloys considered in the current work are shown in Figure 1.

The values of the lattice parameter structures of the ordered $Pt_{0.75}M_{0.25}$ ($M = \text{Fe, Co or Ni}$) alloys considered in the current work are shown in Table 1. This table contains two sets of parameters: the first set are those determined using DFT in the current work, and the second set are experimental values. The values of the lattice constant determined for Pt_xNi_{1-x} in the current work differ nominally from those in the recent studies [30] because of the pseudopotential. In the current work, the pseudopotentials are PAW, whereas, in recent studies, the pseudopotentials were norm-conserving. Because of this, lattice constants in the current work are more accurately estimated; the magnitude of the a parameters estimated in the current work differs from the experimental values by 0.011–0.055 Å, whereas the same parameters differed by 0.082–0.106 Å in [30].

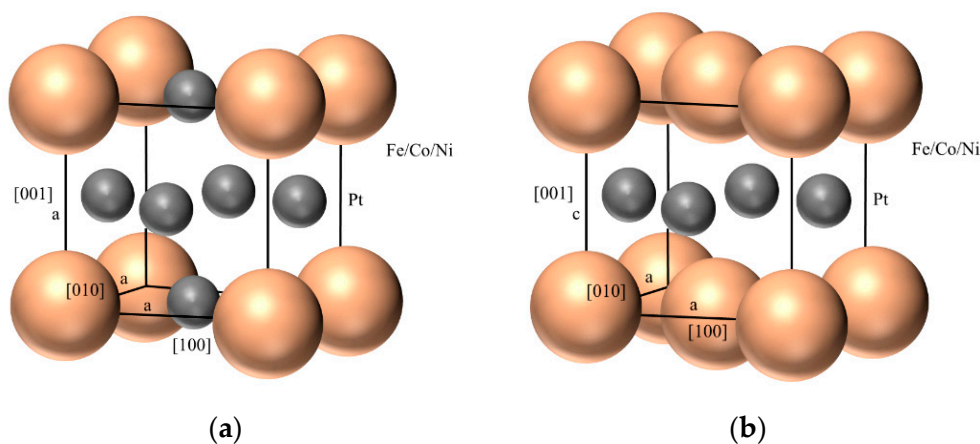


Figure 1. Structures of the ordered (a) L1₂ Pt_{0.75}M_{0.25} (M = Fe, Co or Ni) and (b) L1₀ Pt_{0.5}M_{0.5} alloys. The ordered Pt_{0.25}M_{0.75} alloys are formed by replacing each Pt atom with an M atom and vice versa, in the structure shown in panel (a). The lattice parameters *a* for L1₂ and L1₀ and *c* (for L1₀ only) are shown.

Table 1. Lattice parameters determined in the current work (‘Theory’) for each of the ordered L1₂ Pt_{0.25}M_{0.75} (M = Fe, Co or Ni) and Pt_{0.75}M_{0.25} alloys and for the ordered L1₀ Pt_{0.5}M_{0.5} alloy together with corresponding experimental values (‘Exptl’). The lattice parameters *a* and *c* are defined in Figure 1. All dimensions are in Å.

Alloy	Phase	<i>a</i>		<i>c</i>	
		Theory	Exptl	Theory	Exptl
Pt _{0.75} Fe _{0.25}	L1 ₂	3.911	3.866 [33]	-	-
Pt _{0.50} Fe _{0.50}	L1 ₀	3.894	3.852 [33]	3.705	3.713 [33]
Pt _{0.25} Fe _{0.75}	L1 ₂	3.740	3.750 [33]	-	-
Pt _{0.75} Co _{0.25}	L1 ₂	3.890	3.831 [34]	-	-
Pt _{0.50} Co _{0.50}	L1 ₀	3.817	3.810 [35]	3.727	3.710 [35]
Pt _{0.25} Co _{0.75}	L1 ₂	3.666	3.66 [34]	-	-
Pt _{0.75} Ni _{0.25}	L1 ₂	3.878	3.837 [33]	-	-
Pt _{0.50} Ni _{0.50}	L1 ₀	3.895	3.840 [35]	3.540	3.610 [35]
Pt _{0.25} Ni _{0.75}	L1 ₂	3.657	3.646 [33]	-	-

2.1. Spin-Resolved Electron Band Structures for the Ordered Pt_xM_{1-x} Alloys

The electronic band structures for the ordered Pt_xM_{1-x} (M = Fe, Co or Ni) alloys are shown in Figure 2. The band-resolved exchange splitting $\delta\varepsilon_{\text{ex}j}(k)$ is defined in Equation (1):

$$\delta\varepsilon_{\text{ex}j}(k) = E_{\uparrow;j}(k) - E_{\downarrow;j}(k) \quad (1)$$

where $E_{\uparrow;j}(k)$ and $E_{\downarrow;j}(k)$ are the energies of the spin-up and down bands, respectively, and *j* is the band index. The ordinate *E* of each graph in Figure 2 is defined in Equation (2)

$$E_j(k) = \frac{1}{2}(E_{\uparrow;j}(k) + E_{\downarrow;j}(k)) \quad (2)$$

Using the definitions presented in Equations (1) and (2), the spin-resolved electronic band structures were calculated and are presented in Figure 2.

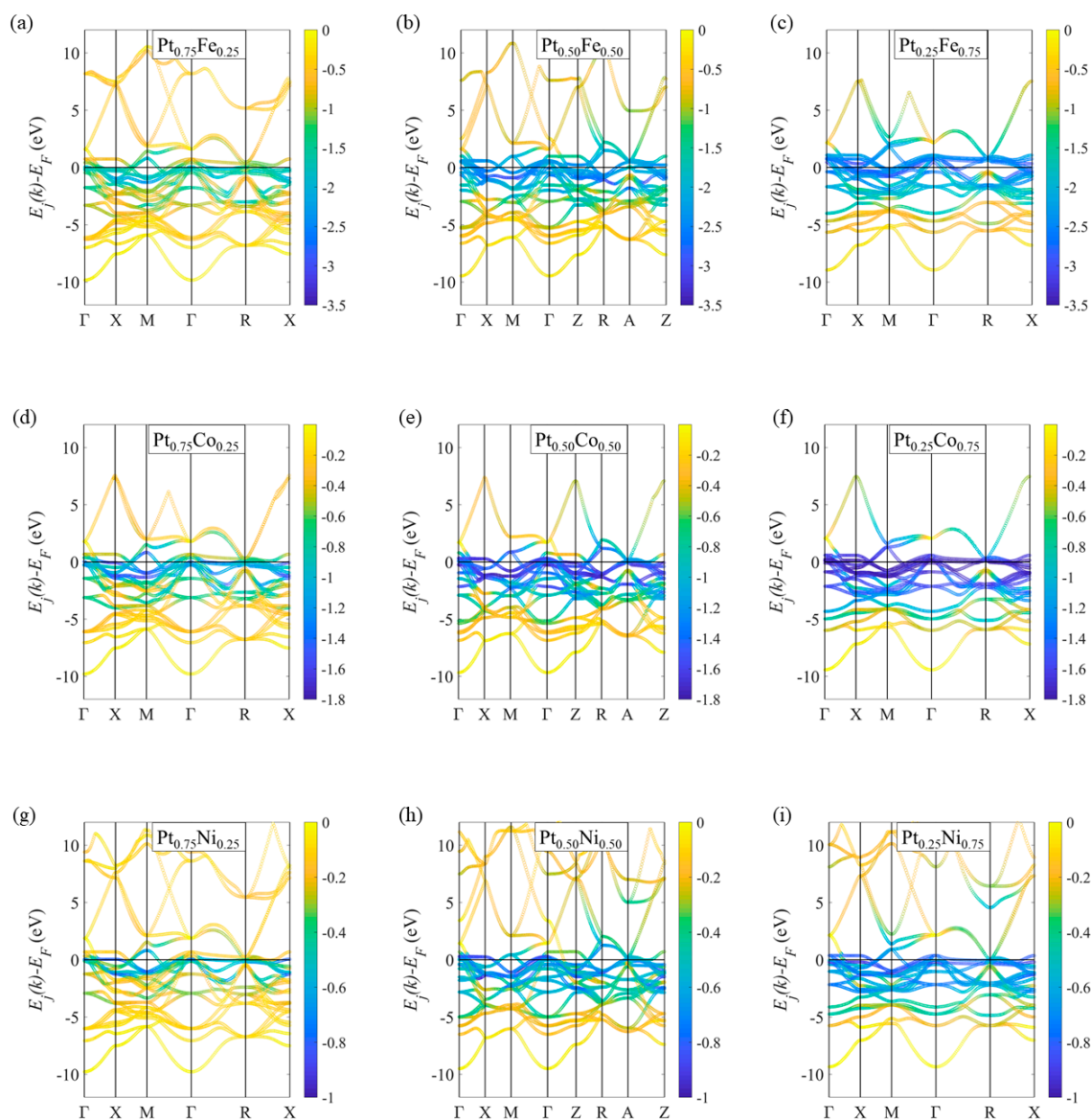


Figure 2. Spin-resolved electronic band structures of the (a–c) $\text{Pt}_x\text{Fe}_{1-x}$, (d–f) $\text{Pt}_x\text{Co}_{1-x}$ and (g–i) $\text{Pt}_x\text{Ni}_{1-x}$ ordered alloys. The $\text{Pt}_{0.50}\text{Fe}_{0.50}$, $\text{Pt}_{0.50}\text{Co}_{0.50}$ and $\text{Pt}_{0.50}\text{Ni}_{0.50}$ alloys are ordered L1_2 structures, whereas the remaining alloys are L1_0 . E_F is the Fermi level, and the legends show the exchange splitting $\delta\varepsilon_{\text{ex}j}(k)$ in eV.

To quantify the spin-polarized dispersions presented in Figure 2, the atomically resolved magnetic moments μ_{Pt} and μ_{M} of the ordered $\text{Pt}_x\text{M}_{1-x}$ ($\text{M} = \text{Fe}, \text{Co}$ or Ni) alloys are presented in Table 2. This analysis was performed in two ways: first, by integrating the projected densities of states (PDOS) and then second, by calculating the Lowdin charges [36]. Both methods show that the Fe, Co and Ni atoms carry the majority of the magnetic moment in each alloy.

Table 2. Magnetic moments μ_{Pt} and μ_M for the Pt and metal (Fe, Co or Ni) atoms, respectively determined in the current work for each of the ordered L1₂ Pt_{0.25}M_{0.75} and Pt_{0.75}M_{0.25} alloys, and for the ordered L1₀ Pt_{0.5}M_{0.5} alloy. The unbracketed and bracketed moments were determined using the Lowdin and projected densities of states (PDOS) methods, respectively (see text). All magnetic moments are in μ_B .

Alloy	Phase	μ_{Pt}	μ_M
Pt _{0.75} Fe _{0.25}	L1 ₂	0.378 (0.388)	3.309 (3.386)
Pt _{0.50} Fe _{0.50}	L1 ₀	0.408 (0.400)	3.007 (3.051)
Pt _{0.25} Fe _{0.75}	L1 ₂	0.401 (0.381)	2.762 (2.677)
Pt _{0.75} Co _{0.25}	L1 ₂	0.337 (0.324)	2.041 (2.135)
Pt _{0.50} Co _{0.50}	L1 ₀	0.423 (0.411)	1.965 (1.908)
Pt _{0.25} Co _{0.75}	L1 ₂	0.406 (0.386)	1.848 (1.838)
Pt _{0.75} Ni _{0.25}	L1 ₂	0.168 (0.161)	0.749 (0.712)
Pt _{0.50} Ni _{0.50}	L1 ₀	0.376 (0.387)	0.792 (0.762)
Pt _{0.25} Ni _{0.75}	L1 ₂	0.360 (0.364)	0.752 (0.764)

2.2. Exchange Splitting ΔE_{ex} for the Ordered Pt_xm_{1-x} Alloys

Within the Stoner model, the contribution of the delocalized component of magnetization to the energies of the spin-up and down bands $E_{\uparrow;j;St}$ and $E_{\downarrow;j;St}$ are given by Equations (3) and (4):

$$E_{\uparrow;j;St}(k) = E_j(k) - I_j(k) \frac{n_{\uparrow;itin;j}(k) - n_{\downarrow;itin;j}(k)}{n_{\uparrow;itin;j}(k) + n_{\downarrow;itin;j}(k)} \quad (3)$$

$$E_{\downarrow;j;St}(k) = E_j(k) + I_j(k) \frac{n_{\uparrow;itin;j}(k) - n_{\downarrow;itin;j}(k)}{n_{\uparrow;itin;j}(k) + n_{\downarrow;itin;j}(k)} \quad (4)$$

where $I_j(k)$ is the k-resolved Stoner parameter and $n_{\uparrow;itin;j}(k)$ and $n_{\downarrow;itin;j}(k)$ are the number of itinerant (or delocalized) spin up and down charge carriers, respectively.

The exchange splitting due to the delocalized magnetic moments can then be evaluated by taking the difference between $E_{\uparrow;j;St}(k)$ and $E_{\downarrow;j;St}(k)$ which gives:

$$\delta\varepsilon_{ex;j;St}(k) = -2I_j(k)m_{j;itin}(k) \quad (5)$$

The normalized magnetic moment $m_{j;itin}(k)$ due to itinerant charge is defined in Equation (6):

$$m_{j;itin}(k) = \frac{n_{\uparrow;itin;j}(k) - n_{\downarrow;itin;j}(k)}{n_{\uparrow;itin;j}(k) + n_{\downarrow;itin;j}(k)} \quad (6)$$

To establish the importance of the Stoner contribution to the total magnetization at each k-point, the total k-resolved exchange splitting is obtained by integrating the band-resolved exchange splitting $\delta\varepsilon_{ex;j;St}(k)$:

$$\Delta E_{ex}(k) = \int_{-\infty}^{E_F} \delta\varepsilon_{ex;j;St}(k) dE \quad (7)$$

The normalized magnetic moment $m_j(k)$ due to all charge is defined in Equation (8):

$$m_j(k) = \frac{n_{\uparrow;j}(k) - n_{\downarrow;j}(k)}{n_{\uparrow;j}(k) + n_{\downarrow;j}(k)} \quad (8)$$

where $n_{\uparrow;j}(k)$ and $n_{\downarrow;j}(k)$ are the total number of spin up and down charge carriers, respectively. The resulting $\Delta E_{ex}(k)$ are shown in Figure 3.

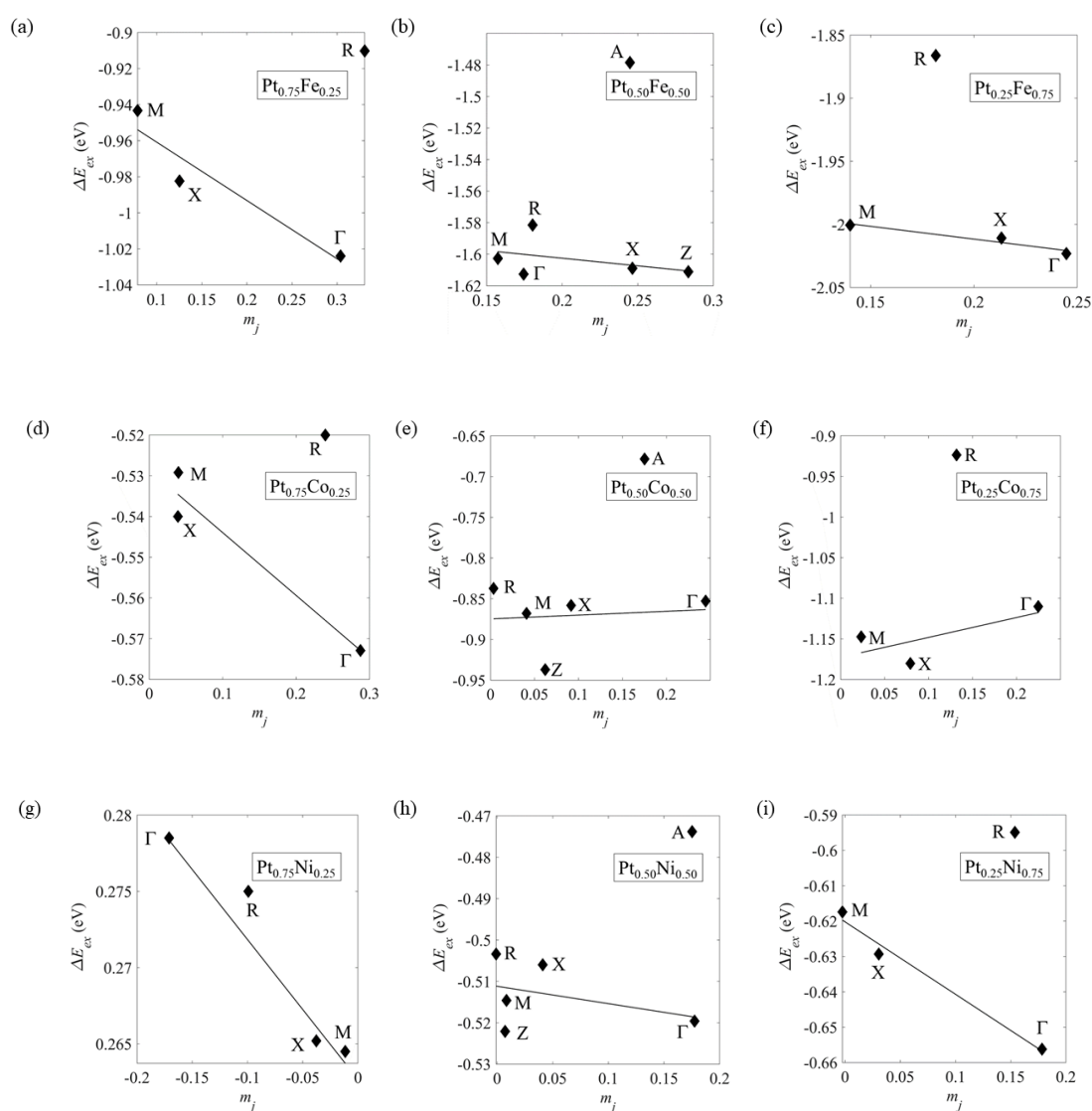


Figure 3. Exchange splitting ΔE_{ex} for the ordered (a–c) $\text{Pt}_x\text{Fe}_{1-x}$, (d–f) $\text{Pt}_x\text{Co}_{1-x}$ and (g–i) $\text{Pt}_x\text{Ni}_{1-x}$ ordered alloys. The labels correspond to high symmetry positions in the electron band structure, and m_j is the normalized total magnetic moment. The line included in each graph is a guide for the eye.

3. Discussion

The primary of this work was primarily the characterization and discussion of the spin-polarized electronic band structures for each of the ordered $\text{Pt}_x\text{M}_{1-x}$ ($M = \text{Fe}, \text{Co}$ or Ni) alloys. Table 1 shows that the geometric model used in the current study is accurate within the levels of approximation used by density functional theory (DFT). This is evidenced by the low (<1%) percentage error in the DFT estimates of a and c compared to their experimental values. The significance of this low level of error between the experimental and theoretical values of a and c supports the choice of pseudopotential and exchange-correlation interaction used in the current simulations and described in full in the ‘Materials and Methods’ section of this work.

Using the equilibrium values of a and c presented in Table 1, the magnetic moments presented in Table 2 were calculated. The values of the magnetic moment in Table 2 show that the magnetic moment of the Pt atoms is consistently lower than the moments of the Fe, Co or Ni atoms. The total magnetic moment per unit cell of each alloy is seen to decrease with increasing Pt concentration.

The spin-resolved electronic band structures shown in Figure 2 demonstrate a similar behavior on alloy composition to those evidenced in Table 2 and discussed in the previous paragraph. For all of the

band structures presented in Figure 2 that contain either Fe or Co, the most magnetic occupied bands lie close to the Fermi level in the region of energy occupied predominantly by d orbitals. This behavior is partially seen for the $\text{Pt}_x\text{Ni}_{1-x}$ alloys. However, in this latter case, the $\text{Pt}_{0.75}\text{Ni}_{0.25}$ alloy is significantly less magnetic than $\text{Pt}_{0.5}\text{Ni}_{0.5}$ or $\text{Pt}_{0.25}\text{Ni}_{0.75}$. This reduces the moment carried by the d-bands.

To gain quantitative insight into the spin-polarized band structures presented in Figure 2 and to establish the relative importance of both localized and itinerant magnetism in these alloys, the total exchange splitting $\Delta E_{\text{ex}}(k)$ was calculated using Equation (7) at each of the high-symmetry points of the electronic band structures presented in Figure 2. Equation (7) will generate values of $\Delta E_{\text{ex}}(k)$ which include contributions from both the itinerant (Stoner) charge and a more localized, non-Stoner charge.

The relative importance of these two components can be determined qualitatively from Figure 3 and is encapsulated by a discussion of the straight lines that have been added to each panel. The gradient and zero-intercepts of these lines depend on the relative contributions to the exchange splitting from itinerant and non-itinerant (or localized) magnetism. A purely itinerant (Stoner) model would predict a straight line that passes through the origin, which not the case for each of the panels in Figure 3. However, each of the lines has a nonzero gradient, so there is some dispersive contribution to the exchange splitting. Consequently, this qualitative analysis shows that each of the alloys contains a mixture of local and non-local magnetism.

To establish a quantitative relationship between the delocalized component of the magnetism and the Stoner parameter requires some assumptions about the Stoner parameter. There is a priori no reason to assume that the Stoner parameter should remain constant with the band or with the k-position. The physical reason for this is because Stoner magnetism arises from an energetic balance between the exchange (Pauli) and the repulsive Coulomb interactions between charge carriers. The net contribution of these terms disperses with both band energy and k, so it may be reasonably expected that $I_j(k)$ may as well. This dispersion is apparent in Figure 3. In particular, it can be seen for the $\text{Pt}_{0.50}\text{Co}_{0.50}$ and the more magnetic $\text{Pt}_{0.25}\text{Co}_{0.75}$ panels; the linearity is complex. In both cases at $m_j < 0.1$, a linear segment appears to exist but will not intersect with points at larger m_j . This complexity discourages a deduction of the Stoner parameter from the data presented in the current work. It does, however, show that the Stoner model is complex for these alloys and that this complexity is dependent on both structure and total magnetism. It is of note that the largest deviation from conventional Stoner magnetism is apparent for the Co-bearing alloys, whose total magnetization lies between that of the Fe- and Ni-bearing alloys. The precise reason for this is, however, not clear.

For both the $L1_2$ and $L1_0$ phases, the R and A points, respectively, lie significantly far from these predictions. This behavior is seen less clearly for the $\text{Pt}_{0.75}\text{Ni}_{0.25}$ alloy though this latter observation is expected to be a consequence of the low magnetic moment seen for this particular phase, which was discussed in the previous paragraphs. The directionality of these deviations is significant. For both the $L1_2$ and $L1_0$ cases, these deviations occur in a direction, which is parallel to the $[111]$ crystalline direction. By considering the real-space alloy structures in Figure 1, this direction has the greatest interatomic direction between nearest-neighbors as the closest pairs of atoms are identical and lie at the fractional $(0,0,0)$ and $(1,1,1)$ positions of the unit cell. Because of the large inter-atomic distance along the $[111]$ direction, it is unlikely that a significant delocalized bond exists between these identical atoms. This reduction in bonding is then plausibly responsible for the significant breakdown of the itinerant model and offers a very convenient insight into the Stoner mechanism. Rather than considering the mechanism as entirely anisotropic, the DFT predictions in the current work have shown that it is more appropriate to consider the delocalization along the binding directions of the crystal. In addition to this, the earlier qualitative analyses have shown that the Stoner parameter is nonconstant throughout k-space, though a model for the parameter is not proposed.

4. Materials and Methods

The density functional theory (DFT) calculations presented in this study were performed using Quantum Espresso [36]. A Brillouin-zone sampling of $(20 \times 20 \times 20)$ was used to accurately model

the delocalized systems considered in this study. A wave-function kinetic energy cutoff of 75 Ry and a charge density/potential cutoff of 300 Ry were also used throughout this work, together with a first-order Methfessel–Paxton smearing of 0.02 Ry [37]. PAW pseudopotentials were used from the pslibrary package [38] to model the core charge density for Pt, Fe, Co and Ni. The PBE-GGA approximation was used throughout this work. In order to ensure convergence of the self-consistent field to the lowest Kohn–Sham energy state, a notably low value of mixing parameter β (0.05) was used.

To obtain the equilibrium lattice parameters a presented in Table 1 for the $L1_2$ structures, the equation of state for each alloy with that structure was calculated, and the minimum of that equation of state determined numerically. The equation of state was obtained by plotting the density functional theory (DFT) Kohn–Sham energy as a function of a . For the $L1_0$ structures, a similar approach was used; however, for each value of a , the lattice was allowed to relax along the c direction. The equilibrium lattice parameters obtained in this way for both the $L1_2$ and $L1_0$ structures were used throughout the remainder of this work. The band structures were subsequently calculated using the equilibrium lattice parameters and the orthogonal unit cells shown in Figure 1.

5. Conclusions

The ordered $L1_2$ and $L1_0$ phases of the binary Pt_xM_{1-x} ($M = \text{Fe, Co and Ni}$; $x = 0.25, 0.50$ and 0.75) alloys were investigated using spin-polarized density functional theory (DFT). The investigations have quantified the magnetic moment of each of these ordered alloys and have shown that the magnetization is strongest in the Fe-carrying alloys and weakest in those containing Ni. The spin-resolved magnetic band-structures for these alloys reflect these quantitative observations and support a model of magnetism that is primarily localized and generated by charge transfer between the d-orbitals.

The k-resolved exchange splitting of each of these alloys was discussed in terms of both localized and itinerant (Stoner) magnetism. A qualitative discussion of these terms has shown that both exist in these ordered alloys. The validity of the Stoner model was discussed qualitatively using an analysis of the exchange splitting at each of the high symmetry points in the electronic band structures for each of the alloys. It was seen that the Stoner parameter is nonconstant across k-space and that itinerant magnetism breaks down extensively at the R (A) points for the $L1_2$ ($L1_0$) structures. It is suggested that charge channeling may be the reason for this failure.

Funding: This research received no external funding.

Conflicts of Interest: The author declares no conflict of interest.

References

1. Singamaneni, S.; Bliznyuk, V.N.; Binek, C.; Tsymbal, E.Y. Magnetic nanoparticles: Recent advances in synthesis, self-assembly and applications. *J. Mater. Chem.* **2011**, *21*, 16819–16845. [[CrossRef](#)]
2. Ferrando, R.; Jellinek, J.; Johnston, R.L. Nanoalloys: From Theory to Applications of Alloy Clusters and Nanoparticles. *Chem. Rev.* **2008**, *108*, 845–910. [[CrossRef](#)] [[PubMed](#)]
3. Li, Y.-Q.; Xu, M.; Dhawan, U.; Liu, W.-C.; Wu, K.-T.; Liu, X.-R.; Lin, C.; Zhao, G.; Wu, Y.-C.; Chung, R.-J. Iron–gold alloy nanoparticles serve as a cornerstone in hyperthermia-mediated controlled drug release for cancer therapy. *Int. J. Nanomed.* **2018**, *13*, 5499–5509. [[CrossRef](#)] [[PubMed](#)]
4. De Jong, W.H. Drug delivery and nanoparticles: Applications and hazards. *Int. J. Nanomed.* **2008**, *3*, 133–149. [[CrossRef](#)] [[PubMed](#)]
5. Krishnan, K.M.; Pakhomov, A.B.; Bao, Y.; Blomqvist, P.; Chun, Y.; Gonzales, M.; Griffin, K.; Ji, X.; Roberts, B.K. Nanomagnetism and spin electronics: Materials, microstructure and novel properties. *J. Mater. Sci.* **2006**, *41*, 793–815. [[CrossRef](#)]
6. Koh, I.; Blois, J. Magnetic Nanoparticle Sensors. *Sensors* **2009**, *9*, 8130–8145. [[CrossRef](#)]
7. Rocha-Santos, T.A. Sensors and biosensors based on magnetic nanoparticles. *TrAC Trends Anal. Chem.* **2014**, *62*, 28–36. [[CrossRef](#)]

8. Neamtu, M.; Nadejde, C.; Hodoroaba, V.-D.; Schneider, R.J.; Verestiuc, L.; Panne, U. Functionalized magnetic nanoparticles: Synthesis, characterization, catalytic application and assessment of toxicity. *Sci. Rep.* **2018**, *8*, 1–11. [[CrossRef](#)]
9. Rossi, L.M.; Costa, N.J.S.; Silva, F.P.; Wojcieszak, R. Magnetic nanomaterials in catalysis: Advanced catalysts for magnetic separation and beyond. *Green Chem.* **2014**, *16*, 2906–2933. [[CrossRef](#)]
10. Rodrigues, T.S.; Da Silva, A.G.M.; Camargo, P.H.C. Nanocatalysis by noble metal nanoparticles: Controlled synthesis for the optimization and understanding of activities. *J. Mater. Chem. A* **2019**, *7*, 5857–5874. [[CrossRef](#)]
11. Massalski, T.B.; Okamoto, H.; Subramanian, P.R.; Kacprzak, L. (Eds.) *Binary Alloy Phase Diagrams*, 2nd ed.; ASM International: Materials Park, OH, USA, 1990; p. 2844. [[CrossRef](#)]
12. Cadeville, M.; Morán-López, J. Magnetism and spatial order in transition metal alloys: Experimental and theoretical aspects. *Phys. Rep.* **1987**, *153*, 331–399. [[CrossRef](#)]
13. Cadeville, M.; Dahmani, C.; Kern, F. Magnetism and spatial order in Ni-Pt and Co-Pt alloys. *J. Magn. Magn. Mater.* **1986**, *54–57*, 1055–1056. [[CrossRef](#)]
14. Sadhukhan, B.; Nayak, A.; Mookerjee, A. Effect of disorder on the optical response of NiPt and Ni₃Pt alloys. *Comput. Mater. Sci.* **2017**, *140*, 1–9. [[CrossRef](#)]
15. Andreatza, P.; Pierron-Bohnes, V.; Tournus, F.; Andreatza-Vignolle, C.; Dupuis, V. Structure and order in cobalt/platinum-type nanoalloys: From thin films to supported clusters. *Surf. Sci. Rep.* **2015**, *70*, 188–258. [[CrossRef](#)]
16. Alam, A.; Kraczek, B.; Johnson, D.D. Structural, magnetic, and defect properties of Co-Pt-type magnetic-storage alloys: Density-functional theory study of thermal processing effects. *Phys. Rev. B* **2010**, *82*, 024435. [[CrossRef](#)]
17. Wen, Y.-H.; Zhang, L.-H.; Wang, J.-B.; Huang, R. Atomic-scale insights into thermal stability of Pt₃Co nanoparticles: A comparison between disordered alloy and ordered intermetallics. *J. Alloys Compd.* **2019**, *776*, 629–635. [[CrossRef](#)]
18. Shuttleworth, I.G. Magnetism in the strained ordered phases of Pt_xFe_{1-x} and Pt_xCo_{1-x} (x = 0.25, 0.5, and 0.75). *J. Phys. Chem. Solids* **2018**, *114*, 153–162. [[CrossRef](#)]
19. Makushko, P.V.; Verbytska, M.Y.; Shamis, M.N.; Verbytska, T.I.; Beddies, G.; Safonova, N.Y.; Albrecht, M.; Makogon, I.M. Effect of initial stress/strain state on the L₁₀ phase formation of FePt in FePt/Au/FePt trilayers. *Appl. Nanosci.* **2019**, *10*, 2775–2780. [[CrossRef](#)]
20. Shuttleworth, I.G. The effects of strain on the ordered phases of Ni_xPt_{1-x} (x = 0.25, 0.5, and 0.75). *Chem. Phys. Lett.* **2017**, *689*, 41–47. [[CrossRef](#)]
21. Zhang, S.; Johnson, D.D.; Shelton, W.A.; Xu, Y. Hydrogen Adsorption on Ordered and Disordered Pt-Ni Alloys. *Top. Catal.* **2020**, *63*, 714–727. [[CrossRef](#)]
22. Zhao, Z.; Fisher, A.; Shen, Y.; Cheng, D. Magnetic Properties of Pt-Based Nanoalloys: A Critical Review. *J. Clust. Sci.* **2016**, *27*, 817–843. [[CrossRef](#)]
23. Karoui, S.; Amara, H.; Legrand, B.; Ducastelle, F. Magnetism: The driving force of order in CoPt, a first-principles study. *J. Phys. Condens. Matter* **2013**, *25*, 056005. [[CrossRef](#)] [[PubMed](#)]
24. Zunger, A.; Wei, S.-H.; Ferreira, L.G.; Bernard, J.E. Special quasirandom structures. *Phys. Rev. Lett.* **1990**, *65*, 353–356. [[CrossRef](#)]
25. Soven, P. Coherent-Potential Model of Substitutional Disordered Alloys. *Phys. Rev.* **1967**, *156*, 809–813. [[CrossRef](#)]
26. Rowlands, D.A.; Ernst, A.; Györfy, B.L.; Staunton, J.B. Density functional theory for disordered alloys with short-range order: Systematic inclusion of charge-correlation effects. *Phys. Rev. B* **2006**, *73*, 165122. [[CrossRef](#)]
27. Staunton, J.B.; Marmodoro, A.; Ernst, A. Using density functional theory to describe slowly varying fluctuations at finite temperatures: Local magnetic moments in Gd and the ‘not so local’ moments of Ni. *J. Phys. Condens. Matter* **2014**, *26*, 274210. [[CrossRef](#)]
28. Guevara, U.; López, R.; Blanco, J.; Núñez, J.; Hernández, U.J.G. Theoretical study of electronic properties and spin density in Pt-Co alloys. *Mater. Res. Express* **2019**, *6*, 096514. [[CrossRef](#)]
29. Alsaad, A.; Ahmad, A.; Qattous, H.A. Structural, electronic and magnetic properties of M_xPt_{1-x}, (M = Co, Ni and V) binary alloys. *Heliyon* **2019**, *5*, e02433. [[CrossRef](#)]
30. Shuttleworth, I.G. The quasiparticle band structures of ordered Ni_xPt_{1-x}. *Heliyon* **2018**, *4*, e01000. [[CrossRef](#)]

31. Pisanty, A.; Amador-Bedolla, C.; Ruiz, Y.; De La Vega, M. Band structures of Ni₃Pt and NiPt₃. *Eur. Phys. J. B* **1990**, *80*, 237–239. [[CrossRef](#)]
32. Yonezawa, F.; Morigaki, K. Coherent Potential Approximation. *Prog. Theor. Phys. Suppl.* **1973**, *53*, 1–76. [[CrossRef](#)]
33. Sternik, M.; Couet, S.; Łażewski, J.; Jochym, P.; Parlinski, K.; Vantomme, A.; Temst, K.; Piekarz, P. Dynamical properties of ordered Fe–Pt alloys. *J. Alloys Compd.* **2015**, *651*, 528–536. [[CrossRef](#)]
34. Pearson, W.B. *A Handbook of Lattice Spacings and Structures of Metals and Alloys*; Pergamon Press Ltd.: Oxford, UK, 1964.
35. Leroux, C.; Cadeville, M.C.; Pierron-Bohnes, V.; Inden, G.; Hinz, F. Comparative investigation of structural and transport properties of L₁₀NiPt and CoPt phases; the role of magnetism. *J. Phys. F Met. Phys.* **1988**, *18*, 2033–2051. [[CrossRef](#)]
36. Giannozzi, P.; Andreussi, O.; Brumme, T.; Bunau, O.; Nardelli, M.B.; Calandra, M.; Car, R.; Cavazzoni, C.; Ceresoli, D.; Cococcioni, M.; et al. Advanced capabilities for materials modelling with Quantum ESPRESSO. *J. Phys. Condens. Matter* **2017**, *29*, 465901. [[CrossRef](#)] [[PubMed](#)]
37. Methfessel, M.; Paxton, A.T. High-precision sampling for Brillouin-zone integration in metals. *Phys. Rev. B* **1989**, *40*, 3616–3621. [[CrossRef](#)] [[PubMed](#)]
38. Corso, A.D. Pseudopotentials periodic table: From H to Pu. *Comput. Mater. Sci.* **2014**, *95*, 337–350. [[CrossRef](#)]

Publisher’s Note: MDPI stays neutral with regard to jurisdictional claims in published maps and institutional affiliations.



© 2020 by the author. Licensee MDPI, Basel, Switzerland. This article is an open access article distributed under the terms and conditions of the Creative Commons Attribution (CC BY) license (<http://creativecommons.org/licenses/by/4.0/>).